IOSR Journal of Mechanical and Civil Engineering (IOSR-JMCE)
e-ISSN: 2278-1684,p-ISSN: 2320-334X, Volume 17, Issue 1 Ser. I (Jan - Feb 2020), PP 01-19
www.iosrjournals.org

Effect of Torsional Restraint Degree and Rigidity of Sections on the behavior of Lateral Loads R.C. cores of Irregular shapes

Akram M. Abdelmaksod[1], Hisham A. El-Arabaty[2], Mohamed N. Fayed[3], Gamal H. Mahmoud[4]

[1] *(Structural Engineering Department, Faculty of Engineering/ Ain-Shams University, Cairo, Egypt)*
[2] *(Structural Engineering Department, Faculty of Engineering/ Ain-Shams University, Cairo, Egypt)*
[3] *(Structural Engineering Department, Faculty of Engineering/ Ain-Shams University, Cairo, Egypt)*
[4] *(Structural Engineering Department, Faculty of Engineering/ Ain-Shams University, Cairo, Egypt)*
Corresponding Author:Akram M. Abdelmaksod

Abstract: *Using reinforced concrete shear walls and cores is one of the most effective systems in resisting lateral loads. Analysis of buildings under the effect of lateral loads is performed using highly sophisticated commercial software finite element analysis packages. In order to account for concrete cracking, the design of these cores is performed using interaction diagrams, based on the relevant code idealization of the strain diagram throughout the section height. This idealization does not consider the torsional movement of these cores in computation of their ultimate capacity. Previous research by the authors studied the difference in behavior between regular and irregular shapes of cores, especially those which have discontinuity in web at load direction. Additionally, an extensive study was conducted to investigate the actual structural behavior of cores of different section shapes, through the development of more accurate nonlinear finite element analysis models, taking into account steel yield, and concrete cracking. In this research, finite element models using concrete damaged plasticity (CDP) had been built; shell elements with layered reinforcing steel were used to simulate the geometry and reinforcing steel of RC cores. An experimental work from the literature including an RC core with T-shaped was used to verify the proposed modeling technique. Then, an extensive parametric study includes non-linear analysis of symmetric and unsymmetrical core shapes was conducted to study the main parameters affecting core behavior. These parameters are: different degrees of torsional rotations on the overall section capacity, width and thickness of core walls. The overall conclusions reached are used to understand the effect of proposed parameters on the behavior of regular and irregular cores. Moreover, important recommendations regarding the "reduction factors" were suggested to adapt the common interaction diagram design procedure, in order to be more realistic in estimating the moment capacity of cores with different torsional restraint degrees, and with different geometrical configuration.*

Keywords:*Finite Element Modeling, Reinforced Concrete cores, Nonlinear analysis, Cracked section analysis*

Date of Submission: 31-12-2019 Date of Acceptance: 15-01-2020

I. Introduction and Problem Description

One of the most effective systems in resisting lateral loads in buildings is the use of reinforced concrete shear walls and cores. They have become widely used among different types of buildings owing to their high moment capacity. Architectural requirements at many situations restrict the allowable places where these elements can be located through the building. This results in either using only one RC core in the building with the columns, or using more than one core. Most of time, structural engineer is forced to use the RC cores at the pre-defined location by the architectural engineer, mainly around elevators and stairs. All these restrictions result in different degrees of torsional rotations for the building in addition to various ratios between section dimensions.

All design software packages do not consider either the degree of torsional restraint applied to the considered RC cores because of its surrounding elements, or the ratio between its dimensions, especially at the case of irregular shapes. The objective of this paper is to study the main parameters affecting the behavior of regular and irregular RC cores, and to propose modifications in the design procedure of theses elements to account for these studied parameters.

(Figure 01) illustrates that the same core may be free to rotate or torsionally restraint by a specific degree according to its location among other elements in a building. For example, the Z-shaped core in (Figure 01-a)is placed as the main element resisting lateral loads in Y-direction in this building; columns share in lateral loads resistance is significantly small according to their low shear stiffness compared to the Z-shaped RC core. This results in allowing the RC core to rotate freely without a significant resistance. On the other hand, placing

other cores and shear walls as in (Figure 02) restrict the torsional rotation of the system which in turn affect the behavior of RC cores.

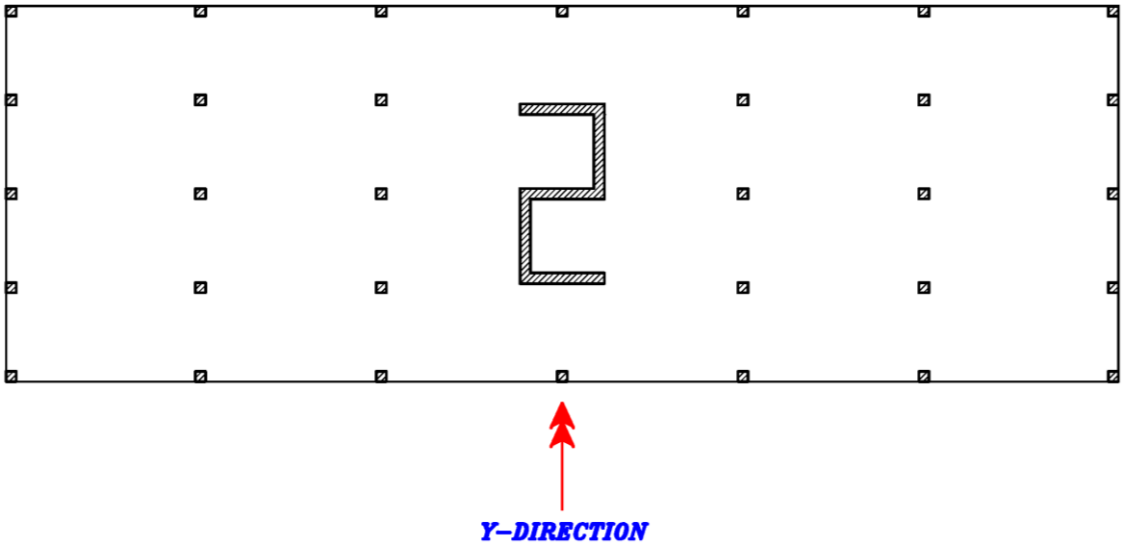

a- A free to rotate Z-shaped core

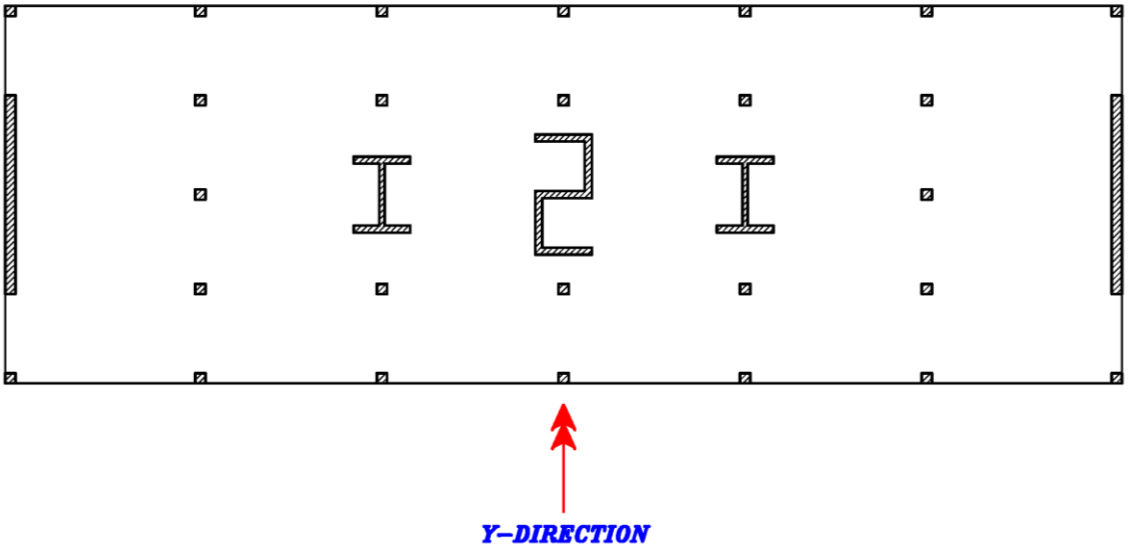

b- Z-shaped core exhibit a degree of torsion restraint

Figure01. Examples of different locations of Z-shaped core

Another point to consider is that any of previous cores may have different configurations which in turn results in bigger or smaller width to thickness ratios of flanges and webs. This may affect the distribution of stresses among the elements resulting in higher variation of stresses through elements perpendicular to the force direction which conflicts with the constant idealization of strains and stresses in these elements assumed by design codes.

The objective of this research is to utilize a more sophisticated non-linear analysis for a group of selected section shapes for RC cores, to make an accurate assessment of the effect of some proposed parameters on core behavior and its moment capacity. These parameters are degree of torsional restraint applied at different levels along core height, discontinuity of web, width of the intermediate flange and its thickness. In addition, the research target is to evaluate the deviation of proposed models to the base model which is a symmetric I-section because of having the closest moment capacity values to traditional commercial software packages.

II. Development of the Nonlinear Finite Element Model

ABAQUS was used as finite element software to perform the analysis in this study. Concrete damaged plasticity (CDP) model was selected to simulate the concrete material from ABAQUS material library. All

concrete material properties in tension and compression were taken as studied and verified by (EL-Arabaty, H.A., Fayed, M.N., Mahmoud, G.H. and Abdelmaksod, A.M., (2019)) in their previous research.

For concrete tension stiffening, the following values had been selected: (σto = 2.65 Mpa), and (ε_{cr} = 0.0000783)) with a linear tension softening relation up to (ε_{tu}=0.10). Whereas, in compression the following data were used: (f'_c = 40.0Mpa), (ε_{c1}= 0.0018), (ε_u= 0.003), and (E_{cm}= 33840 Mpa).

Steel reinforcement materials were modeled using a bilinear elasto-plastic model with strain hardening taken into account, for which the plastic modulus (Esh) was approximately 1% of its initial elastic counterpart. Steel 360/520 was selected withyield stress (fy=360 Mpa), ultimate stress (fu=520 MPa), ultimate strain (ε_u=0.25) andelastic modulus of elasticity (Es=206010 MPa).

III. Verification and Sensitivity Analysis

Concrete damaged plasticity (CDP) was tested and verified by the authors in their previous research (EL-Arabaty, H.A., Fayed, M.N., Mahmoud, G.H. and Abdelmaksod, A.M., (2019))besides the using of shell elements to simulate RC cores with their reinforcing steel. One beam from a series of twelve conventional RC beam specimens tested by (Vecchio& Shim (2004)), and commonly referred to as the 'Toronto series', was used for calibration. Comparison between analytical results and experimental ones showed an acceptable correlation which proved the adequacy of using this proposed technique in modeling RC members.

Another experimental work was selected at this study to assure the efficiency of using shell element in modeling RC cores. As stated previously RC shear walls and cores have become used in the majority of high rise building to resist lateral loads. However, reviewing the previous experimental works done on shear walls showed that most of shear walls in the literature were tested under the effect of cyclic loads. On the other hand, this study concentrates on calculating the moment capacity of different types of cores. This does not need modeling the cores under the effect of cyclic loads; increasing load in one direction is enough to satisfy the requirements of this study. Hencean RC core with T-shaped cross section was selected for calibration. The selected RC core was tested by (Thomsen, J.H. and Wallace, J.W. (2004)). The selected core was tested under the effect of cyclic lateral load, but in this study, the first cycle only was used to verify the proposed modeling technique. Additionally, the same core was verified and modeled using shell elements in ABAQUS by (Feng, D.C., Ren, X.D. and Li, J., (2018)).The dimensions of the tested specimen are shown in (Figure 02-a), whereas the geometrical and reinforcing details of the core cross section are shown in (Figure 02-b). Totally three kinds of reinforcement bars are used in the specimen. First type was No. 2 bars, which have a diameter of 6.35mm and yield strength of 448 MPa; they were used for the distributed horizontal and vertical bars of the wall except at the position of concentration. Additionally, the second type was No.3 bars, which have a diameter of 9.53mm and a yield strength of 414 MPa, are used for the longitudinal bars at connections and ends of the wall. Finally, the smooth wires, which have a diameter of 4.75mm and a yield strength of 448 MPa, are used for the transverse bars and stirrups of the wall.

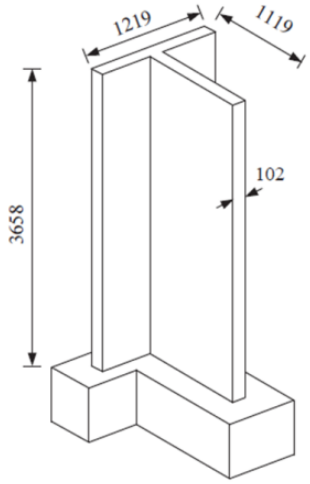

a- Dimensions of the tested RC core

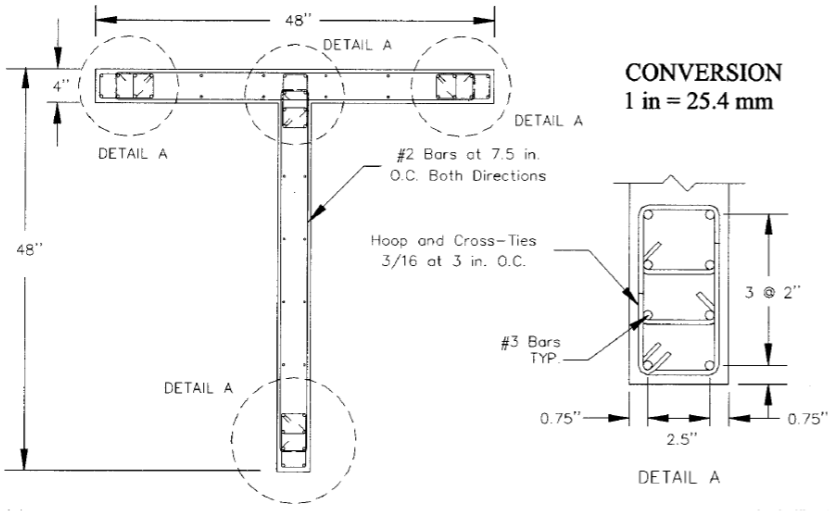

b- Geometrical and reinforcing details

Figure02. Geometry and reinforcing configuration of the tested RC core by (Thomsen, J.H. and Wallace, J.W. (2004))

The design compressive strength for the tested core was 43.6 MPa. Moreover, there was an axial load applied constantly at the top of the core. The axial load and material properties are given in (Table 01)

Specimen	Axial load	Concrete strength	Steel strength		
TW2	730 kN	42.8 MPa	No.2	No.3	Wire
			448 MPa	414 MPa	448 MPa

Table01. Material properties for concrete and reinforcing steel used in the tested RC core

Furthermore, the core specimen was tested in an upright position where a specially fabricated steel load transfer assembly was used to transfer both axial and lateral loads to the wall specimen. Cyclic lateral displacements were applied to the walls by a 556 kN hydraulic actuator mounted horizontally to a reaction wall 3.66 m above the base of the wall. (Figure 03) shows the test setup by (Thomsen, J.H. and Wallace, J.W. (2004)) to study the effect of cyclic load on the behavior of T-shaped core.

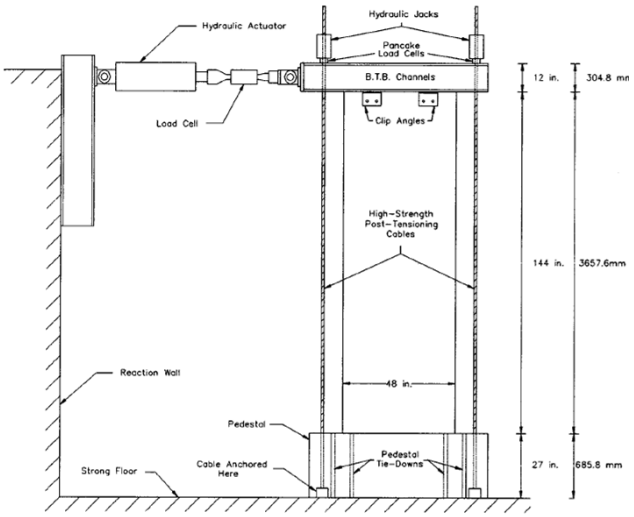

Figure03. Test setup the tested RC core by (Thomsen, J.H. and Wallace, J.W. (2004))

The tested specimen is modeled using (CDP) in ABAQUS with two various techniques. In the first technique, concrete is modeled using four-nodded shell element (S4R), whereas the longitudinal and transversal direction were modeled using rebar layers in shell elements. Spacing (S), and the area (A) which were used to

determine the thickness of the equivalent rebar layer (t=A/S) as well as the angular orientation (α) of the rebar with respect to this local system.In addition, position of the rebars in the shell thickness direction measured from the mid-surface of the shell were specified (positive in the direction of the positive normal to the shell) ABAQUS (2014).

The core was divided into three main parts; first one was the connection between web and flange which has a concentration of longitudinal steel as well as the stirrups. Second part was that one at the ends of flange and webs which also has a concentration of reinforcing steel. Finally, third part was the middle one at the two sides of flange and at the web which has a uniform distribution of both vertical and horizontal reinforcing. Supports had been carried out at end of the lower rigid part to restrain the six degrees of freedom to simulate the fixation conducted at the experimental work. Lateral load had been applied at the top of the core to simulate the applied load in the experimental work. Additionally, in the experiment, an axial load was applied firstly before the application of increasing one directional load, and was held constant during the increments of lateral load.(Figure 04) shows the finite element model using (ABAQUS) software.

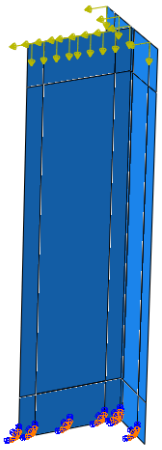

Figure04. Representation of the finite element model for the selected tested T-shaped core

Load-displacement relationship of the analytical and experimental work were studied and illustrated at (Figure 05) which show an acceptable deviation of analytical results to the experimental ones. It is worth to note that the experimental curve is for the first cycle only of applied cyclic load whereas the finite element curve is plotted until the same displacement at the end of the first cycle of cyclic load. It means that the modeled core resist higher loads which are not plotted at this comparison. The model was found to fail at a lateral load equals 450 kN.

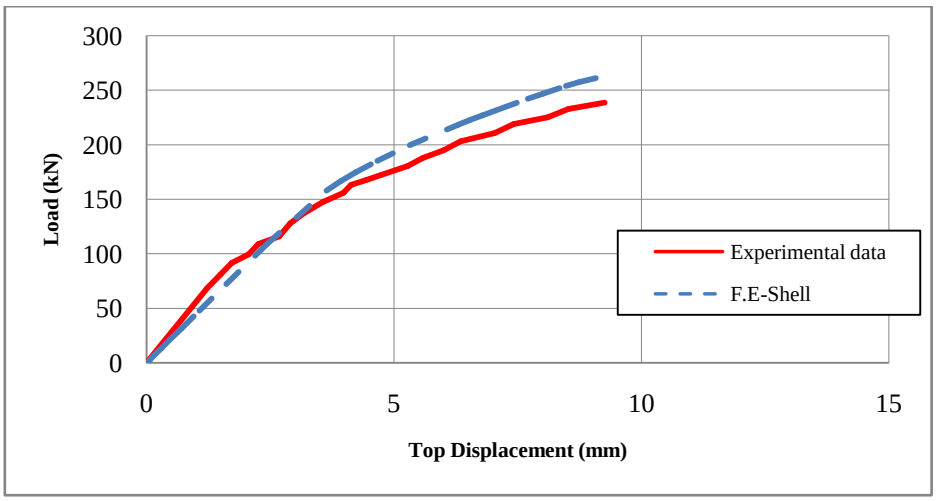

Figure05. Comparison between load-displacement relationship from finite element modeling and from experimental work for the tested RC core

The calibration showed that the difference between analytical and experimental work did not exceed 10% which is an acceptable deviation. At the displacement at end of cycle one in the experiment, the experimental load was 260kN, while the analytical laod at the same displacement scored 239kN. After verification of the previous core specimen which show an acceptable agreement with the captured behavior and results of experimental work. It is provedthat modeling RC members with shell elements using (CDP) in ABAQUS achieves a high degree of accuracy which enables this technique of modeling to be used at this study. Thus, the study of behavior of RC cores under the effect of lateral load is conducted using this verified technique.

IV. Structural Behavior of Regular and Irregular Cores

The study plan for this research involves the simulation of RC cores of regular and irregular shapes under the effect of lateral loads, the main target of this research is to assess the effect of many parameters on the ultimate moment capacity for cross sections of these cores, as compared to that obtained by the traditional interaction diagram assumptions utilized by commercial software packages.

Models of cantilever cores fixed at the base were developed and subjected to lateral forces at the free end of the cantilever. Simulation of the base fixation by preventing all deformation at the points of fixation was found to result in local stress concentrations at points around the fixation, thus stopping the nonlinear analysis runs prematurely, and affecting the overall estimated lateral force, and thus the estimated section moment capacity.

A different simulation for the ground fixation was performed by(EL-Arabaty, H.A., Fayed, M.N., Mahmoud, G.H. and Abdelmaksod, A.M., (2019)) by adding a segment of the same core section but with higher wall thicknesses to provide a relatively rigid segment at below the base level. At the bottom of this rigid segment, fixation is achieved through Zero deformation restraints. This modification in the original model worked out as the failure at ultimate load occurred in the original segment, right at the top of the rigid segment, thus eliminating the effect of possible local stress concentrations. Several models were developed for the proposed study. All models are cantilevers with a height of 15 meters.

A group (1) of three models had been proposed to study the impact of different parameters regarding concrete dimensions and steel reinforcement. The three models are identical in concrete dimensions and steel reinforcement; however, they are different in arrangement of walls along the section. The first section (I-section) is totally symmetrical with continuous web. In addition, second section with unsymmetrical arrangement and with continuous web was proposed in the shape of (E-section). Finally, (Z-section) represents a polar symmetrical section with web discontinuity. The three suggested models with different proposed studied parameters are shown in (Figure 06).

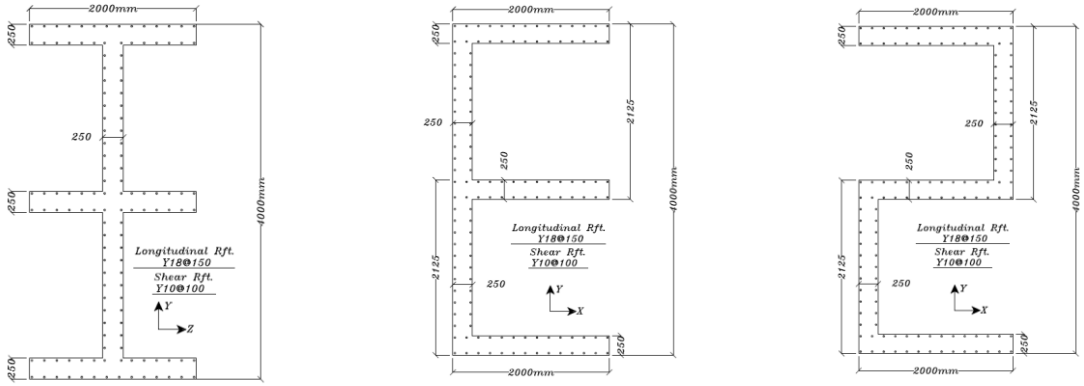

(I-Shape) (E-Shape) (Z-Shape)

Figure06. Concrete dimensions and steel reinforcement for (I, E, and Z models) in group (1) Cross sections to study the degree of torsional restraint

Cores usually exist in buildings which include other structural elements. These elements serve to provide some degree of rotational restraint to the concrete floors, which in turn reduce the torsional rotation of the core sections. The degree of restraint depends on the stiffness and locations of these elements. Three restrained degrees were applied to each model in addition to the free to rotate case. This was implemented by applying torsional moments at three levels along core height which are 5.0 m, 10.0 m and 15.0 m to restrain the torsional rotation of the core at its top to three specific values. These values are +0.01 radians (positive sign means at the direction of its free rotation case), -0.01 radians (negative sign means at the opposite direction of its

free rotation case) and zero radians which means that core is totally restrained at its top. Thus simulates the effect of structural elements surrounding the core, and forcing its in-plane rotation to a specific value by fixing the slab in place. (Table 02) shows the degree of torsional restraint for each type.

MODEL	**I or E or Z**			
Type	A	B	C	D
In-plane rotation restraint	Free to rotate	Specific torsional rotation = + 0.01 radians	Fully restrained in-plane rotation	Specific torsional rotation = - 0.01 radians

Table02. Specifications of models in (group 1) used to study the effect of torsional restraint degree.

Concrete is modeled using four-nodded shell element (S4R). First letter in element name (S) indicates its type which is shell, second one defines the number of points which are four in shell elements, and finally, third letter refers to the type of integration whether it is a full or reduced integration. Reduced integration was selected at this study, so the third letter is (R). (S4R) shell element has six degrees of freedom at each node; three displacements, and three rotations.

Reduced integration uses a lower-order integration to form the element stiffness. The mass matrix and distributed loadings use full integration, despite of using full or reduced integration in element type. Reduced integration reduces running time, especially in three dimensions, and also reduces the file size as well. Elements with reduced integration are also referred to as uniform strain or centroid strain elements with hourglass control. Second-order reduced-integration elements in ABAQUS/Standard generally yield more accurate results than the corresponding fully integrated elements. However, for first-order elements the accuracy achieved with full versus reduced integration is largely dependent on the nature of the problem.

In ABAQUS/Standard thick shells are needed in cases where transverse shear flexibility is important and second-order interpolation is desired. When a shell is made of the same material throughout its thickness, this occurs when the thickness is more than about 1/15 of a characteristic length on the surface of the shell, such as the distance between supports for a static case. Most of tested specimens have a shell thickness less than 1/15 of the beam span; however, thick shell was selected to take into consideration transverse shear flexibility to achieve more accuracy.

Transverse shear stiffness for shell elements in ABAQUS is computed by matching the shear response for the shell to that of a three-dimensional solid for the case of bending about one axis. The transverse shear stiffness of the section of a shear flexible shell element is defined in ABAQUS as:

$\overline{K}_{\alpha,\beta}^{ts} = f_b K_{\alpha,\beta}^{ts}$ (10)

Where;

α, β : are the components of the section shear stiffness in the local directions associated with the shell section definition,

f_b : is a dimensionless factor that is used to prevent the shear stiffness from becoming too large in thin shells,

$K_{\alpha,\beta}^{ts}$: is the actual shear stiffness of the section (calculated by Abaqus or user-defined).

The dimensionless factor f_b is defined in equation (11) as:

$f_b = \frac{1}{1+0.25\ x\ 10^{-4}\frac{A}{t^2}}$ (11)

Where A is the area of the element and t is the thickness of the shell.

When a general shell section is used and the section stiffness is given directly, the $\overline{K}_{\alpha,\beta}^{ts}$ are defined in equation (12) as:

$K_{11}^{ts} = K_{22}^{ts} = \left(\frac{1}{6}(D_{11} + D_{22}) + \frac{1}{3}D_{33}\right)Y,\ K_{12}^{ts} = 0$(12)

Where D_{ij} is the section stiffness matrix, and Y is the initial scaling modulus. The transverse shear stiffness should be specified as the initial, linear elastic stiffness of the shell in response to pure transverse shear strains. For a homogeneous shell made of a linear, orthotropic elastic material, where the strong material direction aligns with the element's local 1-direction, the transverse shear stiffness should be

$K_{11}^{ts} = \frac{5}{6}G_{13}\,t,\ \ K_{22}^{ts} = \frac{5}{6}G_{23}\,t,\ \ K_{12}^{ts} = 0$(13)

G_{13}, G_{23} : are the material's shear moduli in the out-of-plane direction. The number 5/6 is the shear correction coefficient that results from matching the transverse shear energy to that for a three-dimensional structure in pure bending.

Steel reinforcement at the longitudinal and transversal directions were modeled using rebar layers in shell elements. Concentrated point load is acting at the center of gravity of core cross section at level +15.00 at Y direction. Fixation support is applied at level -2.00 which is the end of rigid body by restraining the three transitional degree of freedoms (Ux, Uy, and Uz) for all nodes. Tie constraint is used to contact the core with the rigid body using full contact at all nodes. In addition, coupling constraint is used to connect the point at which

lateral load is acting to all points in its ZY plane with constraint degree of freedoms (Uy, Uz, and Rx). Static, Riks analysis had been performed to get the failure load for the model and consequently, the moment capacity which is the target of this study. Representation for model of I-shaped core is shown in (Figure 07) as an example.

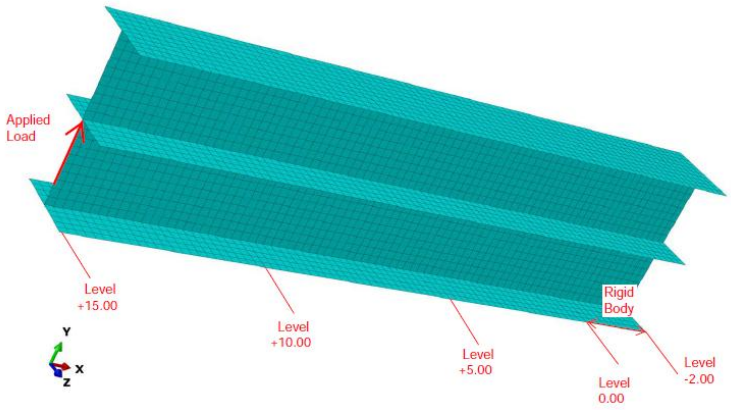

Figure07. Representation of finite element model for model of I-shaped core

The three previous models were adjusted to study the effect of another two parameters on the core behavior and the section moment capacity. The suggested parameters are: the width of intermediate flange and the thickness of same flange. (Figure 08) illustrates the (group 2) three modified models to study the impact of the proposed parameters, and furthermore, it shows theses variable parameters. Additionally, (Table 03)illustrates the properties for each model.

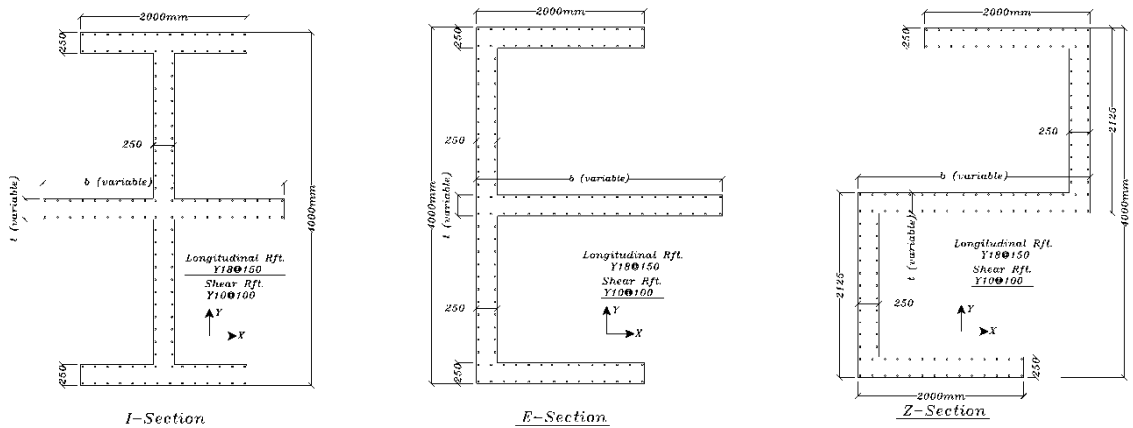

(I-Shape) (E-Shape) (Z-Shape)

Figure08. Concrete dimensions and steel reinforcement for (I, E, and Z models) in (group 2) Cross sections to study the width and thickness of intermediate flange

Proposed models to study the effect of intermediate flange width (Group 2-a)	**MODEL**	**I or E or Z**		
	Type	A	B	C
	Intermediate Flange Thickness	250mm	250mm	250mm
	Intermediate Flange Width	2000mm	3000mm	4000mm
Proposed models to study the effect of intermediate flange thickness (Group 2-b)	**MODEL**	**I or E or Z**		
	Type	A	B	C
	Intermediate Flange Thickness	250mm	350mm	500mm
	Intermediate Flange Width	2000mm	2000mm	2000mm

Table03. Properties for (I, E and Z) models in (group 2) to study the effect of width and thickness of the intermediate flange

V. Results and Discussion

6.1 Stress and strain contours

(Figure09)illustrates the stresses and strains obtained for a sample analysis run (I-section) in (group 1) with the free to rotate case (Type A). As shown, the variation of stresses and strains before cracking is uniform, with equal maximum strain values occurring at the top and bottom points of the section. The same applies to the stress variation. Moreover, it is obvious that compressive stresses are concentrated at the connections between flange and web while they exhibit a significant decrease toward the free end of flange. This behavior resembles the rigidity of the middle part of flange compared to its free part.

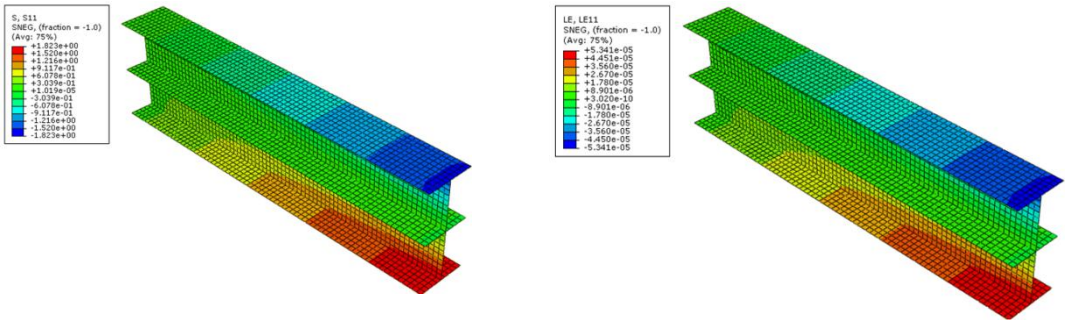

a) Stress contours b) Strain contours

Figure09. Stress and strain contours at longitudinal direction (before cracking) for (I-section) model in (group 1) with free to rotate case (Type A)

When cracking starts to occur, the behavior starts changing and the strain variation shows a maximum tensile value at the section bottom higher than the maximum compressive value at the section top point, which means that the Neutral axis has started to move upward as shown in (Figure 10-a). Accompanying this change, a similar change in the stress diagram occurs, where yield stress starts to dominate the tensile zone (Figure 10-b), and extend upward more and more as the load increases and the section approaches failure. The results show that the model is simulating the actual concrete/steel section behavior accurately.

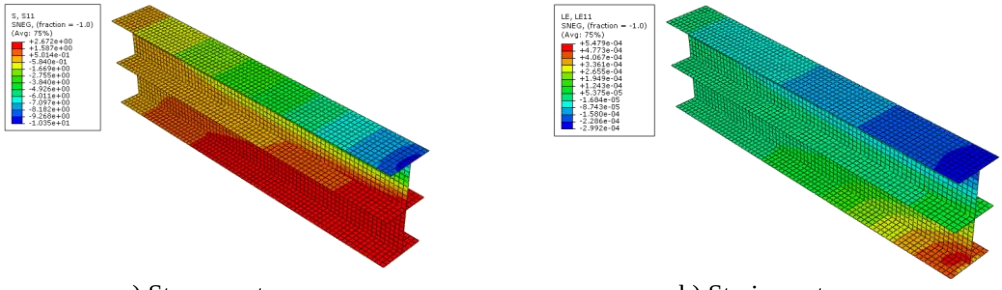

a) Stress contours b) Strain contours

Figure10. Stress and strain contours at longitudinal direction (after cracking) for (I-section) model in (group 1) with free to rotate case (Type A)

6.2 Effect of torsional restraint degree

To begin with, stresses along the section of (I-shaped) R.C. core obtained from the nonlinear analysis of the four studied model types at the failure stage are shown at (Figure 11). It is obvious that stresses, for all torsional restraint degrees, are almost the same, except small transition for maximum compressive stresses to edges of top flange according to the small torsional rotation. This can be explained by the symmetrical shape of section as continuous web produces a clear compression zone at the section top, where concrete reached crushing limit, while yield strains cover the bottom zone of the section. The small transition of compressive stress is because of the small applied torsional rotation at types B and D.

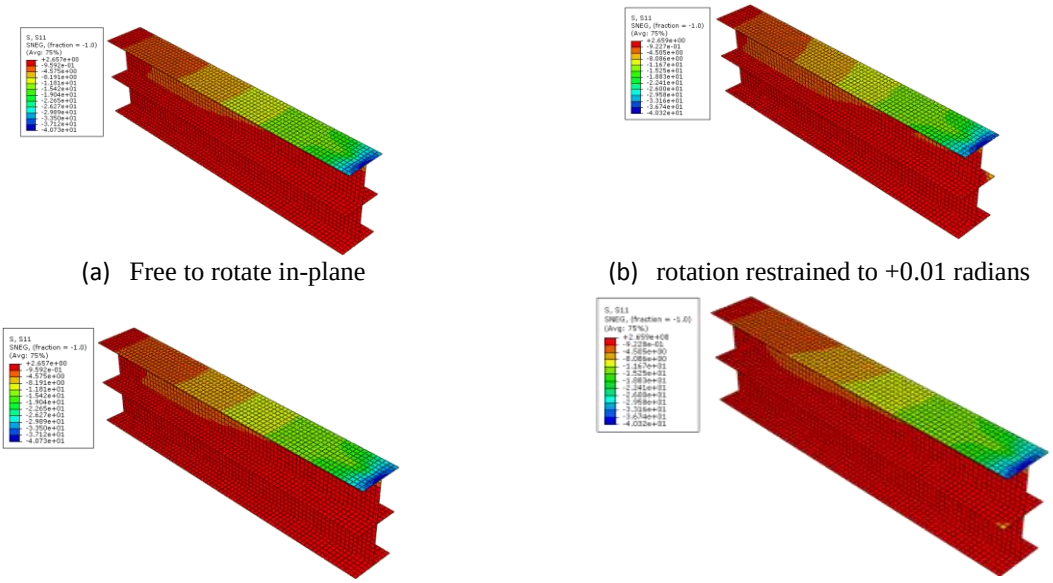

(a) Free to rotate in-plane (b) rotation restrained to +0.01 radians

(c) In-plane rotation totally restrained (d) rotation restrained to -0.01 radians

Figure11. Stress contours (at failure stage) for (I-Section) modelsin group (1)

Moreover, ultimate load capacity and flexural capacity of I-section core remained almost the same for the four types: A, B, C and D. The values of ultimate load and section moment capacity were summarized and tabulated at (Table 04). No major reduction in moment capacity was observed for "torsionally restrained" I-section because of its symmetrical behavior.

MODEL	**I-Section**			
Model Type	A	B	C	D
In-plane rotation restraint	Free to rotate	Rotation restrained to + 0.01 radians	Fully restrained in-plane rotation	Rotation restrained to - 0.01 radians
In-plane rotation at top level of core (radians)	0	+0.01	0	-0.01
In-plane displacement at load direction at top level of core (mm)	72	82	72	82
Ultimate applied load (kN)	2277	2250	2277	2250
Ultimate moment capacity (MN.m)	34.1	33.75	34.1	33.75
Percentage of reduction in capacity compared to I section free to rotate	0	1%	0	1%

Table04. Ultimate moment capacity and in-plane rotation for (I-section) models in (group 1)

Additionally, stress contours through the E-section for the four different types had been studied and illustrated at (Figure 12). Stress contours for all torsional restraint degrees models: B, C, and D, were almost the same, but they differed to stress contours for the free to rotate case. A clear difference had been captured through types B, C, and D which is the increase of part at top flange covered with compressive stresses by moving from +0.01 radians model to -0.01 radians model. This can be clarified by the restrained torsional rotation since the section was free to rotate at type A where it undergoes a high rotation with two types of stresses at the top flange. Then moving to the torsional rotation restrained to +0.01 radians, it undergoes a smaller torsional rotation, which in turn decreased the existence of two types of stresses through top flange, and also dominated the global behavior of section formingonly compressive stress at top flange. The final stress distribution is a combination between the global flexure behavior with only compressive stress at top flange and the torsional restraint behavior with two types of stresses at the same flange. Previous clarification indicates that increasing torsional restraint degree dominates the global flexure behavior and minimizes the torsional behavior. This is followed by zero rotation case, then the -0.01 radians, where flange exhibits only to compressive stresses. Thus, E-section for all restrained rotation degrees behaves in a way relatively close to the I-section.

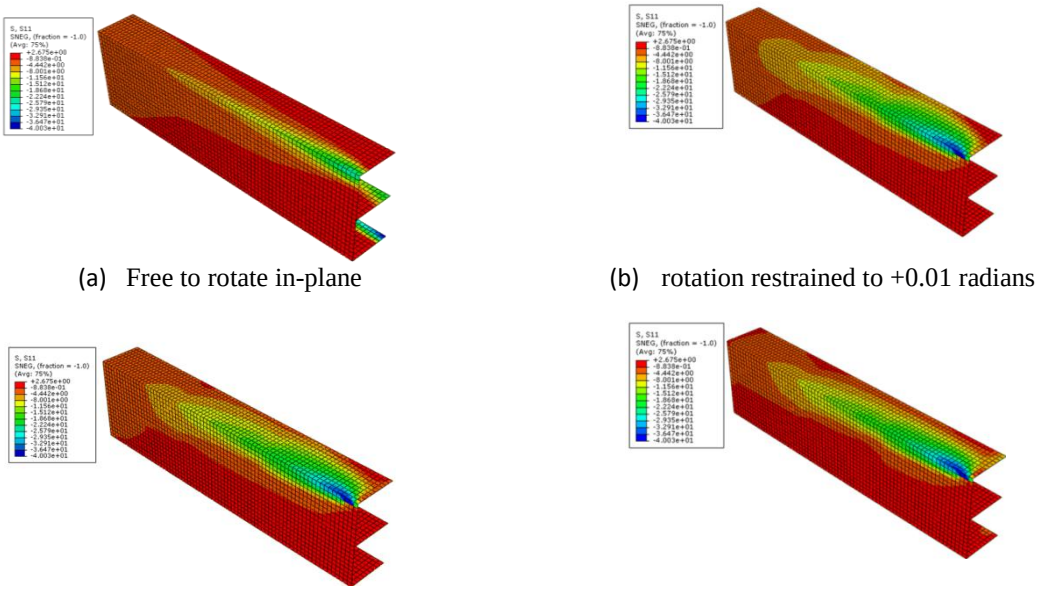

(a) Free to rotate in-plane (b) rotation restrained to +0.01 radians

(c) In-plane rotation restrained (d) rotation restrained to -0.01 radians

Figure12. Stress contours (at failure stage) for (E-Section) modelsin group (1)

Moreover, (Table 05) illustrates the values of ultimate load besides the flexure capacity of all E-section models. All degrees of torsional restraint, E-section exhibit almost the same reduction in moment capacity compared to I-section which is an insignificant reduction. This means that E-section behaves as similar as the I-section provided that its torsional rotation is restrained or even partially restrained. On the other hand, free to rotate case exhibits a 33% reduction in section moment capacity.

MODEL	**E-Section**			
Model Type	A	B	C	D
In-plane rotation restraint	Free to rotate	Rotation restrained to + 0.01 radians	Fully restrained in-plane rotation	Rotation restrained to - 0.01 radians
In-plane rotation at top level of core (radians)	0.101	+0.01	0	-0.01
In-plane displacement at load direction at top level of core (mm)	187	110	105	102
Ultimate applied load (kN)	1530	2220	2240	2270
Ultimate moment capacity (MN.m)	22.9	33.3	33.6	34.05
Percentage of reduction in capacity compared to I section free to rotate	33%	2.3%	2%	0.3%

Table05. Ultimate moment capacityfor(E-section) models in (group 1)

As for Z-section, change in stress contours can be seen in (Figure 13) from the free to rotate case (a) to the three restrained cases (b,c and d). Restraining torsional rotation changes the formation of maximum compressive stress from the top of lower web to the top flange. In addition, it can be seen in (Table 06) that the ultimate capacity for the "torsionally restrained" cases has been reduced relative to the reference capacity of the I-section; however, the three restrained cases achieved almost the same reduction. This can be explained by the effect of the discontinuous web of the section, producing different compression and tension zones in both of the section webs.

More reduction in ultimate moment capacity is observed for the case of the "torsionally unrestrained" case (Model a), reaching a value of 24.0 MN.m which is 30% less than the capacity of the reference I-section. This reduction is a result of 2 factors acting together, namely the discontinuity of the web, and the torsional movement of the section.

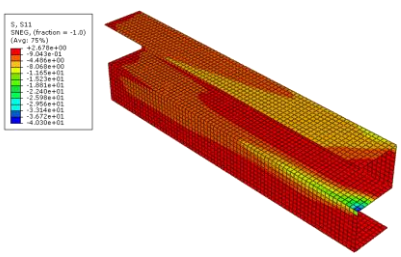

(a) Free to rotate in-plane

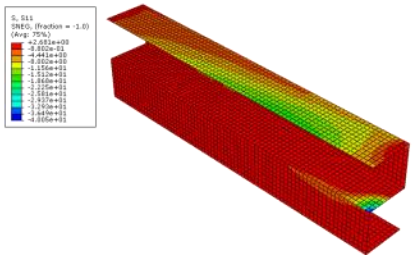

(b) rotation restrained to +0.01 radians

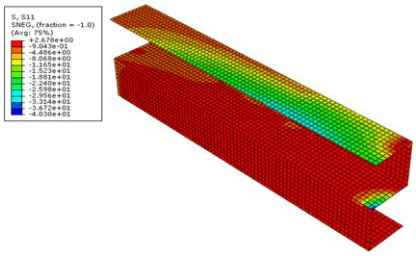

(c) In-plane rotation restrained

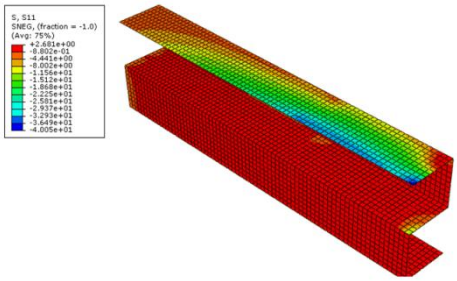

(d) rotation restrained to -0.01 radians

Figure13. Stress contours (at failure stage) for (Z-Section) modelsin group (1)

MODEL	**Z-Section**			
Model Type	A	B	C	D
In-plane rotation restraint	Free to rotate	Rotation restrained to + 0.01 radians	Fully restrained in-plane rotation	Rotation restrained to - 0.01 radians
In-plane rotation at top level of core (radians)	0.042	+0.01	0	-0.01
In-plane displacement at load direction at top level of core (mm)	182	151	81	75
Ultimate applied load (kN)	1600	2060	2100	2070
Ultimate moment capacity (MN.m)	24.0	30.9	31.5	31.05
Percentage of reduction in capacity compared to I section free to rotate	30%	9.3%	8%	8.9%

Table06. Ultimate moment capacity for (Z-Section) modelsin group (1)

6.3 Effect of intermediate flange width

Firstly, the three models of I section had been analyzed using structural parameters shown in (Table 03). Stresses along the section of (I-shaped) R.C. core obtained from the nonlinear analysis are shown at (Figure 14). It is obvious that stress distribution along the section is almost the same for the three models; however, neutral axis location has exhibited small translation downward by increasing the length of intermediate flange.

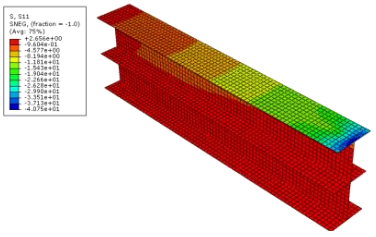

(a) 2000mm Intermediate flange

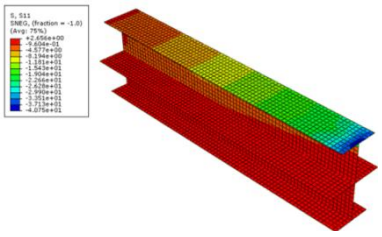

(b) 3000mm Intermediate flange

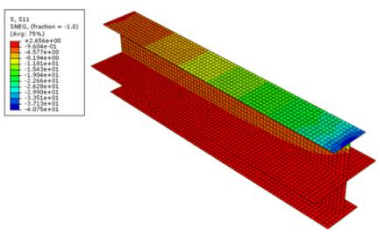

(c) 4000mm Intermediate flange

Figure14. Stress contours (at failure stage) for (I-Section) models in (group 2-a)

Ultimate failure load and flexure capacity of core had been studied; obtained values are almost the same for the three models with a small increase in capacity by increasing intermediate flange width although the R.C area of cross section and the reinforcement area were increased. To investigate this observation, two points had been selected; one of them at the middle of flange whilst the other one at the edge of it. Relation of tensile stress at steel for these two points was plotted with respect to the applied lateral force at (Figure 15).

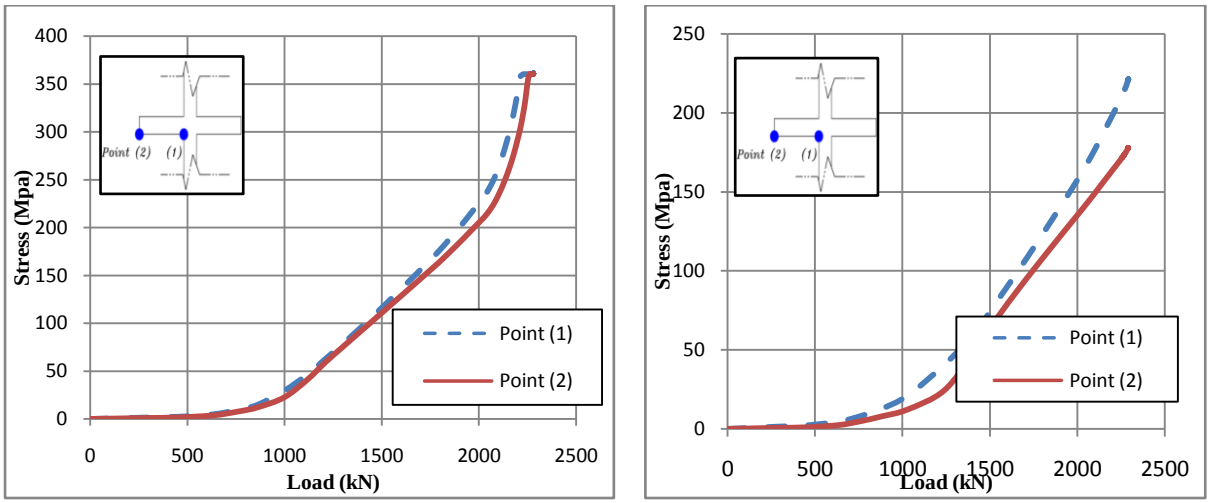

(a) 2000mm Intermediate flange (b) 4000mm Intermediate flange

Figure15. Relationship of reinforcement steel tensile stress through the intermediate flange for I-Section

Previous figures reveal two points. First one is that point (2) located at the edge of flange exhibits a tensile stress smaller than point (1) at the same load step which proves the inadequacy of the assumption of equal stress at the same points in the direction perpendicular to load owing to the shear lag phenomenon which previously discussed and verified by (Zhang, Z. and Li, B., (2017)) and (Chaudhari, S.V. and Chakrabarti, M.A.(2012)). The second point to consider is that diagrams show clearly that with increasing of intermediate flange width, tensile strains and stresses at this flange were decreased. This leads to a smaller share in the flexure capacity of the section; that is why the flexure capacity remained almost the same despite width of intermediate flange in addition to reinforcement were increased.

Secondly, the three models of E section had been analyzed using structural parameters shown in (Table 03). Stresses along the section of (E-shaped) R.C. core obtained from the nonlinear analysis are shown at (Figure 16). Similar to the previous results obtained for I-section, distribution along all parts of section except the intermediate flange is almost the same for the three models; however, neutral axis location at web had exhibited a translation downward by increasing intermediate flange width. Furthermore, compressive stresses had been increased at the free end of intermediate flange with a larger part of flange subjected to compressive stresses. This can be clarified by the increasing in flange flexibility due to increasing its width. Another reason to consider, center of area had been translated far from the shear center of the section by increasing flange width which consequently affects the torsional behavior of section resulting in higher compressive stresses at intermediate flange.

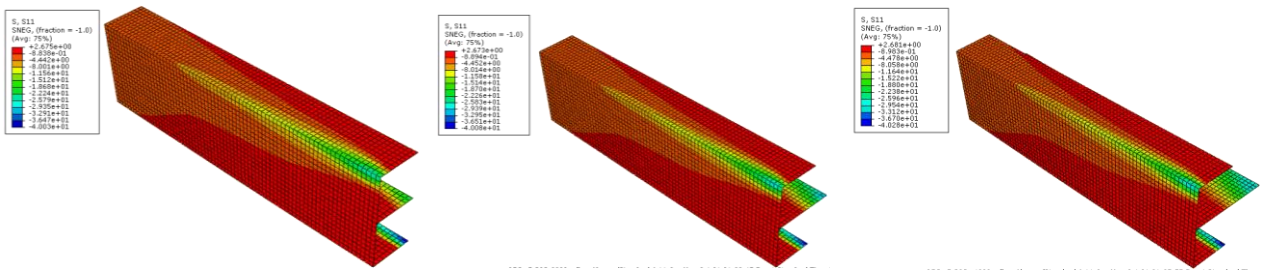

(a) 2000mm Intermediate flange (b) 3000mm Intermediate flange (c) 4000mm Intermediate flange

Figure16. Stress contours (at failure stage) for (E-Section) models in (group 2-a)

Moreover, E section exhibits a significant reduction in ultimate failure load and moment capacity as it was found that moment capacity decreased by 12.4% in case of 4000mm flange compared to 2000mm flange in

spite of increasing section area and reinforcement steel area. This reduction was investigated, and it was found to occur due to two main reasons. First one, strain diagrams, plotted at (Figure17), show that increasing intermediate flange width was accompanied by reduction in areas exposed to yielding steel tensile strains and stresses especially at the web and lower flange whereas it was predicted for all points to be exposed to yielding strain or higher values as the case of 2000mm flange. This results in a smaller share of tensile forces in section flexure capacity. Second reason, increasing of intermediate flange width results in smaller values of tensile strains themselves and stresses at this flange. This leads to also an ineffective share in the flexure capacity of the section.

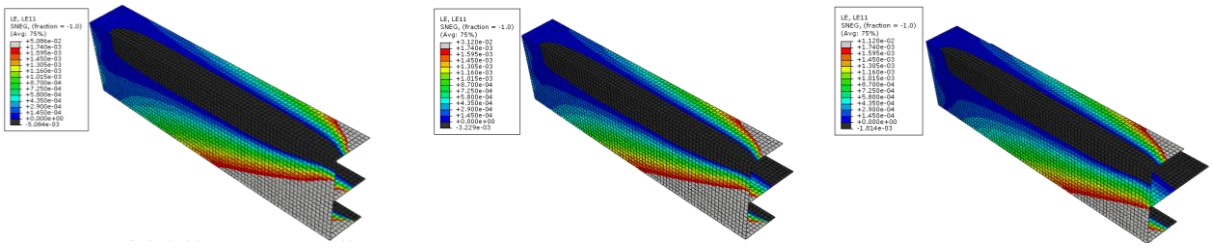

(a) 2000mm Intermediate flange (b) 3000mm Intermediate flange (c) 4000mm Intermediate flange

Figure17. Strain diagram (at failure) in longitudinal direction for E-Section models in (group 2-a)

Finally, the three models of Z section with different widths for the intermediate flange had been analyzed using structural parameters shown in (Table 03). Stresses along the section of (Z-shaped) R.C. core obtained from the nonlinear analysis are shown at (Figure 18). The figure shows that area covered with tensile stresses at intermediate flange through the longitudinal direction of the core were increased by increasing intermediate flange width. This observations show tendency of the two parts of section (each part is the web connected to an outer flange and a part of the intermediate flange) to behave separately as disconnected parts by forming higher more tensile stresses at the intermediate flange. That is because when distance between the two webs was small "Rigid intermediate flange", section tried to behave as a single unit in bending in spite of the web discontinuity which oblige the two parts to behave separately, whilst in the case of large distance between the two webs "Flexible intermediate flange", this distance helps the section to have separate behavior between its two parts.

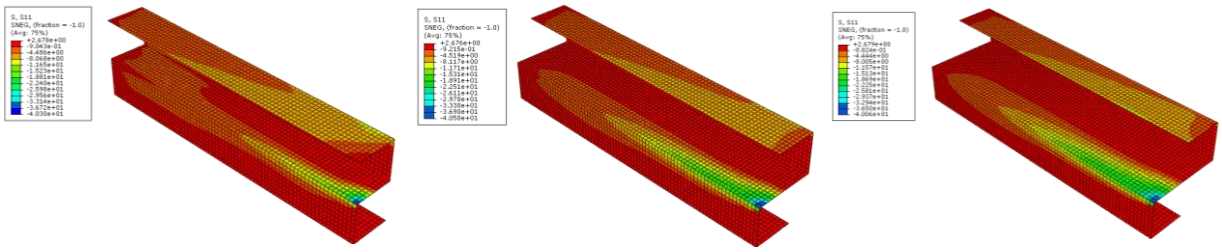

(a) 2000mm Intermediate flange (b) 3000mm Intermediate flange (c) 4000mm Intermediate flange

Figure18. Stress contours (at failure stage) for (Z-Section) models in (group 2-a)

In addition, Z-section showed a significant reduction in moment capacity by increasing intermediate flange widthbecause a reduction reaching 8% was noticed in case of 4000mm intermediate flange compared to the case of 2000mm intermediate flange in spite of increasing section area and reinforcement steel area. The reduction was found to depend on the separation distance between the two webs. For small separation distance "Rigid intermediate flange", section tried to behave as one unit forming compressive stress at the top flange and tensile stresses at the bottom one, but due to web discontinuity smaller values of tensile stresses were formed at bottom of the upper web. On the other hand, for large separation distance "Flexible intermediate flange", effect of web discontinuity appeared quite obviously because tensile stresses formed at bottom of the upper web exceeded those formed at bottom of the lower one. (Figure 19) shows tensile stresses at the bottom of each web. Previous observations prove that increasing intermediate flange width increases the effect of web discontinuity which results in turn into significant reduction in moment capacity.

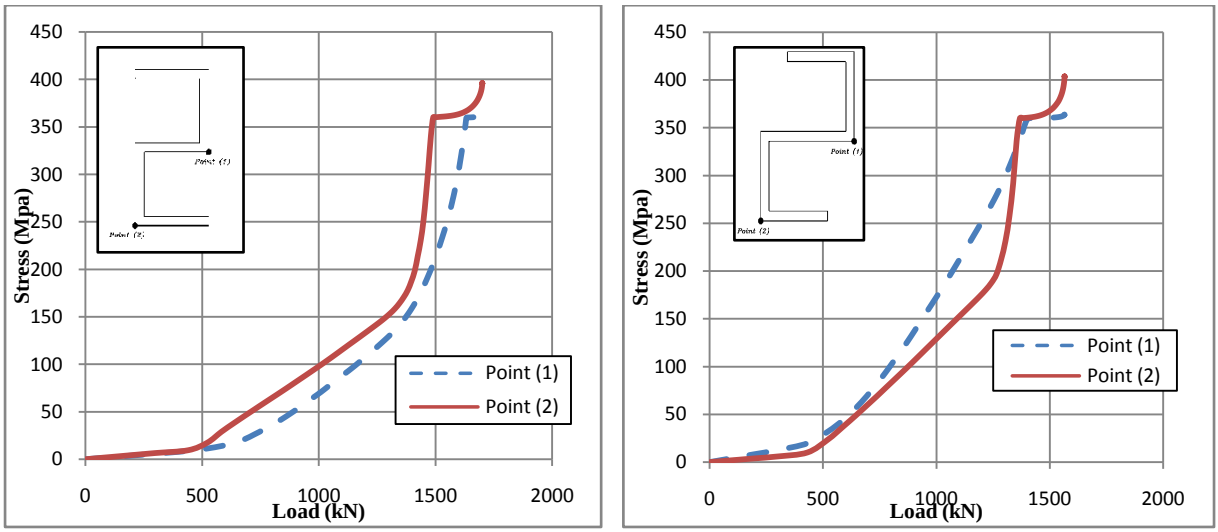

(a) 2000mm Intermediate flange (b) 4000mm Intermediate flange

Figure19. Relationship of reinforcement steel tensile stress at points 1 and 2 for Z-Section

Finally, failure load and moment capacity for the 9 models studied to investigate the effect of intermediate flange width were extracted from ABAQUS analysis and tabulated at (Tables 07, 08 and 09).

MODEL	**I**		
Type	A	B	C
Intermediate Flange Length	2000mm	3000mm	4000mm
Ultimate applied load (kN)	2277	2280	2290
Ultimate moment capacity (MN.m)	34.1	34.2	34.35
Percentage of magnification or reduction in capacity compared to I section with 2000mm intermediate flange	0	+0.30%	+0.73%

Table07.Ultimate moment capacity for I-Section models in (group 2-a)

MODEL	**E**		
Type	A	B	C
Intermediate Flange Length	2000mm	3000mm	4000mm
Ultimate applied load (kN)	1530	1503	1340
Ultimate moment capacity (MN.m)	22.9	22.54	20.1
Percentage of magnification or reduction in capacity compared to E section with 2000mm intermediate flange	0%	-1.57%	-12.4 %

Table08. Ultimate moment capacity for E-Section models models in (group 2-a)

MODEL	**Z**		
Type	A	B	C
Intermediate Flange Length	2000mm	3000mm	4000mm
Ultimate applied load (kN)	1600	1540	1473
Ultimate moment capacity (MN.m)	24.0	23.1	22.1
Percentage of magnification or reduction in capacity compared to Z section with 2000mm intermediate flange	0%	-3.75 %	-8 %

Table09. Ultimate moment capacity for Z-Section models in (group 2-a)

6.4 Effect of intermediate flange thickness

To begin with, three models of I-section using structural properties showed previously at (Table 05) had been analyzed. Stresses at failure stage along the section of (I-shaped) R.C. core obtained from the nonlinear analysis are shown at (Figure 20). No obvious difference was noted between the three analyzed models, and neutral axis also was found at the same location through cross section. The reason of this similarity is that intermediate flange at failure stage is fully cracked without any share of its concrete in flexure capacity.

Another reason to add is that however position of the two rows of reinforcement inside intermediate flange is changed by increasing flange thickness, their center is still at the middle of flange for all studied thicknesses.

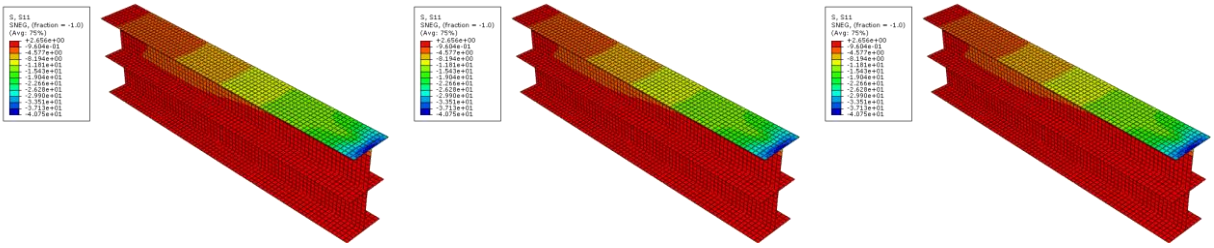

(a) 250mm Intermediate flange thickness (b) 350mm Intermediate flange thickness (c) 500mm Intermediate flange thickness

Figure20. Stress contours (at failure stage) for (I-Section) models in (group 2-b)

As a result of correspondence between sections of different intermediate flange thicknesses in stress distribution, ultimate failure load and moment capacityare almost same for the three models.

For E-section, the three proposed models of E section with different thicknesses of the intermediate flange had been analyzed using structural parametersshown at (Table 03). Stresses along the section of (E-shaped) R.C. core obtained from the nonlinear analysis are shown at (Figure 21). Similar to the previous results obtained for I-section, it is clear that stress distribution along all parts of section except the intermediate flange is almost the same for the three models. Compressive stresses had been increased at the free end of intermediate flange with a larger part of flange subjected to compressive stresses. A reasonable clarification for this observation is that center of area had been translated far from the shear center of the section by increasing flange width which consequently affects the torsional behavior of section resulting in higher compressive stresses at intermediate flange.

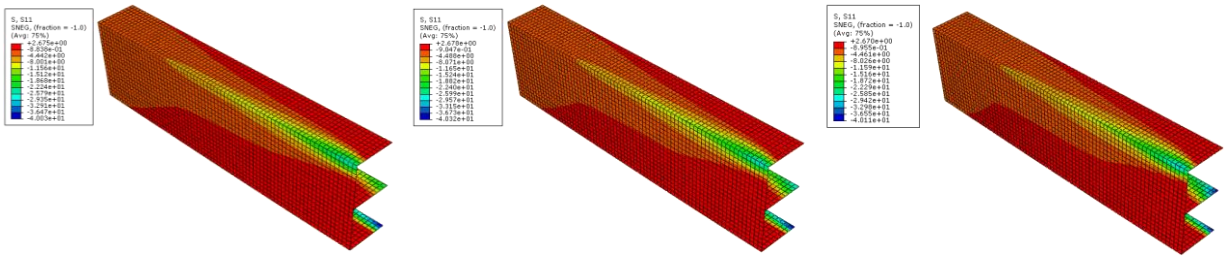

(a) 250mm Intermediate flange thickness (b) 350mm Intermediate flange thickness (c) 500mm Intermediate flange thickness

Figure21. Stress contours (at failure stage) for (E-Section) models in (group 2-b)

Ultimate failure load and moment capacity of core had been studied; a significant rise in flexure capacity as same as the failure load was noticed which was about 22.4% in case of 500mm flange thickness. Section capacity increases due to the higher stresses resulted from higher steel strains in case of 500mm flange thickness compared to the case of 250mm thickness.

To verify the reason of increasing tensile strains, displacements at wall directions of core section was analyzed and plotted at (Figure 22). It was found that they were increased by increasing flange thickness. Not only were the displacements increased, but also rotation of core section at a height of 15m was increased. Previous displacements and rotations clarify why tensile strains of steel had been increased at higher intermediate flange thickness resulting in higher moment capacity. Moreover, displacement at the direction of intermediate flange had been increased from 78mm at 250mm flange thickness to 100mm at 500mm flange thickness, which illustrate the reason of higher compressive stresses at intermediate flange in case of 500mm thickness compared to 250mm thickness which results in lower tensile stresses at the intermediate flange connection with web. However, the increasing of tensile stresses at the lower part of section outweighs the effect of decreasing tensile stresses at the connection between intermediate flange and web. These high tensile stresses at bottom of the section share significantly in calculating the moment capacity. Although section with bigger intermediate flange thickness exhibits relatively higher values of rotations, displacements in wall directions result in higher stresses and in its turn higher capacity.

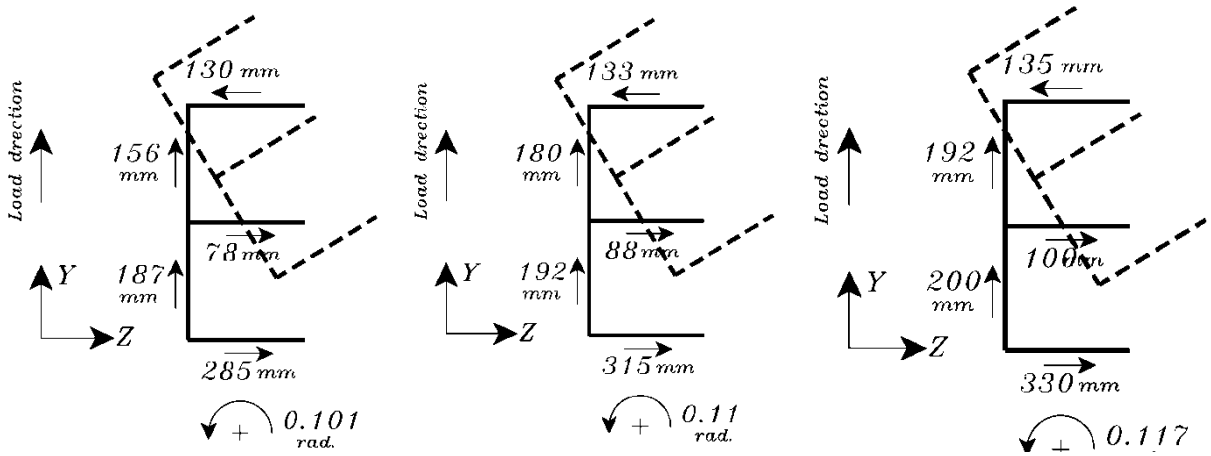

(a) 250mm Intermediate flange thickness (b) 350mm Intermediate flange thickness (c) 500mm Intermediate flange thickness

Figure22. Displacements at walls direction and rotations (at failure) for E-Section models in (group 2-b)

Finally, the three models of Z section with different thicknesses for the intermediate flange had been analyzed using structural parameters at (Table 03). Stress distribution shown at (Figure 23) indicates that areas covered with tensile stresses through lower web of the core were increased by increasing intermediate flange thickness. This describes the tendency of section to behave as one part instead of behaving as two individual parts which leads to decreasing tensile stresses for the upper web and the part of intermediate flange connected to it, and increase tensile stresses at the lower web and its connected lower flange.

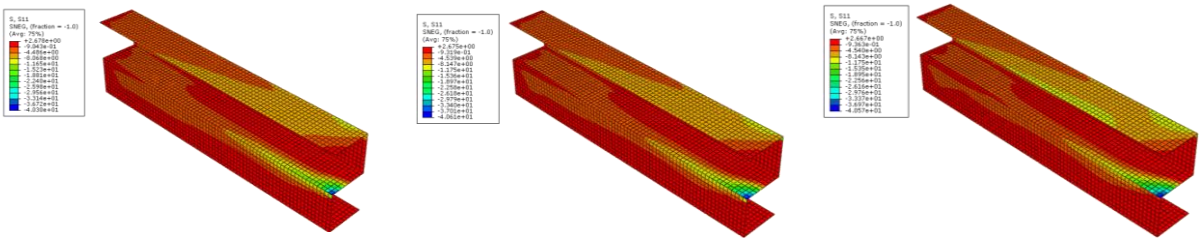

(a) 250mm Intermediate flange thickness (b) 350mm Intermediate flange thickness (c) 500mm Intermediate flange thickness

Figure23. Stress contours (at failure stage) for (Z-Section) models in (group 2-b)

Furthermore, strain contours along sections of the three models were investigated to confirm the previous proposed behavior. (Figure 24-c) illustrates that at the case of 500mm intermediate flange thickness "Rigid intermediate flange", and at the step when steel tensile strain at bottom point of the upper web reached the yielding strain, the majority of lower web strains were found that they had achieved the yielding strain. On the other hand, (Figure 24-a) shows the case of 250mm intermediate web "Flexible intermediate flange". At this case when steel tensile strain of bottom point of the upper web reached the yielding strain, steel yielding strain was found to be achieved at smaller areas of the lower web compared to the case of 500mm intermediate flange thickness. (Figure 24-b) indicates that the case of 350mm flange thickness undergoes an intermediate behavior between the two previous cases.

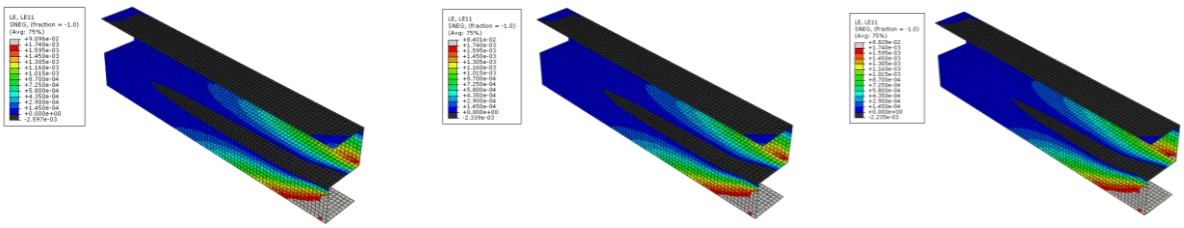

(a) 250mm Intermediate flange thickness (b) 350mm Intermediate flange thickness (c) 500mm Intermediate flange thickness

Figure24. Strain diagram (at failure) in longitudinal direction for (Z-Section) models in (group 2-b)

Z-section exhibits a significant increase of 20% in moment capacity by increasing intermediate flange thickness from 250mm to 500mm. This shows that increasing flange thickness increases its rigidity which in turn raises the tendency of section to behave as one unit. This decreases the effect of web discontinuity and increase moment capacity of the section.

Finally, failure load and moment capacity for the 9 models studied to investigate the effect of intermediate flange thickness were extracted from ABAQUS analysis and tabulated at (Tables 10, 11 and 12).

MODEL	**I**		
Type	A	B	C
Intermediate Flange thickness	250mm	350mm	500mm
Ultimate applied load (kN)	2277	2281	2285
Ultimate moment capacity (MN.m)	34.1	34.2	34.3
Percentage of magnification or reduction in capacity compared to I section with 250mm intermediate flange thickness	0	+0.30%	+0.60%

Table10. Ultimate moment capacity for I-Section modelsin (group 2-b)

MODEL	**E**		
Type	A	B	C
Intermediate Flange Length	250mm	350mm	500mm
Ultimate applied load (kN)	1530	1650	1870
Ultimate moment capacity (MN.m)	22.9	24.75	28.05
Percentage of magnification or reduction in capacity compared to E section with250mm intermediate flange thickness	0%	+8%	+22 %

Table11. Ultimate moment capacity for E-Section modelsin (group 2-b)

MODEL	**Z**		
Type	A	B	C
Intermediate Flange Length	250mm	350mm	500mm
Ultimate applied load (kN)	1600	1780	1935
Ultimate moment capacity (MN.m)	24.0	26.73	29.03
Percentage of magnification or reduction in capacity compared to Z section with 250mm intermediate flange thickness	0%	+11.25 %	+20.95 %

Table12. Ultimate moment capacity for Z-Section modelsin group (2-b)

VI. Summary and Conclusions

- In this research, the main factors affecting the behavior of regular and irregular RC cores were studied. These factors are: the degree of torsional restraint, the intermediate flange width and its thickness. A practical range of torsional rotation and wall dimensions had been applied on modelsto investigate the effect of the suggested factors on the moment capacity of RC cores.
- ABAQUS was used to perform a sophisticated nonlinear finite element analysis for the analysis of reinforced concrete cores under the effect of lateral loads. Verification of the proposed model is performed using published experimental data from an RC core with T-shaped cross section tested under the effect of lateral loads, and the model results were found to be in a high agreement with experimental results.
- For symmetric regular RC core sections:
    - Finite element analysis reveals that the structural behavior of symmetric regular core sections (I-section, etc) is almost the same regardless of the applied degree of torsional rotation because they achieve the same moment capacity under different proposed torsional rotations.Additionally, strain diagram along section height is the most adequate relationship among all studied sections to the full-height linear strain assumption specified by design codes, and applied in commercial software packages.
    - Results obtained from parametric study proved that intermediate flange dimensions have a minimal effect on the moment capacity predicted for these sections. Thus, increasing or decreasing the rigidity of intermediate flange does not improve the behavior.
- For irregular RC core sections:
    - Structural behavior and the resulting stress and strain distribution are highly different at the free to rotate case compared to different rotationally restrained cases, especially at sections with discontinuous webs (Z section, etc). The effect on the ultimate moment capacity of the section is

found to be significant, and reached up to 46% reduction in capacity for some sections which are free to rotate.

- However, the proposed rotationally restrained degrees undergo an improved behavior with a smaller reduction factor. This means that if the building exhibit a small rotational value by fixing the rotation of the buildings using other lateral loads resisting elements, RC cores with irregular shapes will undergo a close moment capacity to those or regular shapes with the same dimensions and reinforcing configuration. It is concluded that the maximum reduction factor for rotationally restrained sections is 9.3% compared to a symmetric section of same dimensions and reinforcement.
- Parametric study showed that irregular core shapes, especially where the section web is discontinuous, depend significantly on the rigidity of intermediate flange.
- Moment capacitiesof these sections increase by 22% in case of continuous webs and 21% in case of discontinuous webs by doubling the ratio of thickness to width. On the other hand, sections have a reduction up to 12.5% in case of continuous webs and 8% in case of discontinuous webs by decreasing the thickness to width ratio of intermediate flange to half of its value.

- Finite element analysis reveals the inadequacy of the linear strain assumption throughout the whole section height which prevents any assessment of the effect of web discontinuity, and any other irregularity in shape. This indicates a critical deficiency in the code assumptions on which commercial software packages base their design routines.
- Non-linear analysis showed the inadequacy of uniform stress distribution for all points at the same line perpendicular to applied load owing to the shear lag. A reduction of 40% in stresses occursbetween points connected to web and free ones at the same flange. This means a smaller share in the moment capacity compared to the calculations done by the commercial software packages.
- A main recommendation is reached in this study regarding the necessity for introducing capacity reduction factors to the computed ultimate moment capacity of core sections under different levels of applied normal force.

References

[1]. ABAQUS Manual, ABAQUS Version 6.11.
[2]. ACI Committee, American Concrete Institute and International Organization for Standardization, 2008. Building code requirements for structural concrete (ACI 318-08) and commentary. American Concrete Institute.
[3]. CEN (ComitéEuropéen de Normalisation). 2004. Eurocode 2: Design of Concrete Structures – Part 1: General Rules and Rules for Buildings, EN 1992-1-1:2004. Brussels:CEN. 230 p.
[4]. Chaudhari, S.V. and Chakrabarti, M.A., 2012. Modeling of concrete for nonlinear analysis using finite element code ABAQUS, International Journal of Computer Apllications, Volume 44 (7), pp.14-18.
[5]. ECP 203 (2012), "Egyptian Code of Practice for Design and Construction of Reinforced Concrete Structures 2012.".
[6]. Ellobody, E. and Young, B., 2011. Numerical simulation of concrete encased steel composite columns. Journal of Constructional Steel Research, 67(2), pp.211-222.
[7]. EL-Arabaty, H.A., Fayed, M.N., Mahmoud, G.H. and Abdelmaksod, A.M., 2019. Finite Element Modeling of lateral loads resisting R.C. cores of Irregular shapes.IOSR Journal of Mechanical and Civil Engineering (IOSR-JMCE), Volume 16, Issue 1, pp.12-27.
[8]. Feng, D.C., Ren, X.D. and Li, G., 2018. Cyclic behavior modeling of reinforced concrete shear walls based on softened damage-plasticity model, Engineering Structures, 166, pp. 363–375.
[9]. Genikomsou, A.S. and Polak, M.A., 2015. Finite element analysis of punching shear of concrete slabs using damaged plasticity model in ABAQUS. Engineering Structures, 98, pp.38-48.
[10]. Hillerborg, A., Modéer, M. and Petersson, P.E., 1976. Analysis of crack formation and crack growth in concrete by means of fracture mechanics and finite elements. Cement and concrete research, 6(6), pp.773-781.
[11]. Hordijk, D.A., 1991. Local approach to fatigue of concrete (Doctoral Dissertation, Delft University of Technology)
[12]. Lubliner, J., Oliver, J., Oller, S. and Onate, E., 1989. A plastic-damage model for concrete. International Journal of solids and structures, 25(3), pp.299-326.
[13]. Moharram, M., 2018. Inelastic Behaviour of Hybrid Reinforced Concrete Beam and Steel Column Systems. (Doctoral Dissertation, Imperial College of Science, Technology and Medicine, London,).
[14]. Thomsen, J.H., and Wallace, J.W., 2004. Displacement-Based design of slender reinforced concrete structural walls—experimental verification, StructEng, 130 (4), pp. 618-630.
[15]. Vecchio, F.J. and Shim, W., 2004. Experimental and analytical reexamination of classic concrete beam tests. Journal of Structural Engineering, 130(3), pp.460-469.
[16]. Zhang, Z. and Li, B., 2016. Seismic performance assessment of Slender T-Shaped reinforced concrete walls, EarthquakeEng, 25, pp. 1-28.

Akram M. Abdelmaksod,et.al. "Effect of Torsional Restraint Degree and Rigidity of Sections on the behavior of Lateral Loads R.C. cores of Irregular shapes". *IOSR Journal of Mechanical and Civil Engineering (IOSR-JMCE)*, 17(1), 2020, pp. 01-19.